

# Multiple Atlas Construction From A Heterogeneous Brain MR Image Collection

Yuchen Xie, Jeffrey Ho, and Baba C. Vemuri\*, *Fellow, IEEE*

**Abstract**—In this paper, we propose a novel framework for computing single or multiple atlases (templates) from a large population of images. Unlike many existing methods, our proposed approach is distinguished by its emphasis on the sharpness of the computed atlases and the requirement of rotational invariance. In particular, we argue that sharp atlas images that retain crucial and important anatomical features with high fidelity are more useful for many medical imaging applications when compared with the blurry and fuzzy atlas images computed by most existing methods. The geometric notion that underlies our approach is the idea of manifold learning in a quotient space, the quotient space of the image space by the rotations. We present an extension of the existing manifold learning approach to quotient spaces by using invariant metrics, and utilizing the manifold structure for partitioning the images into more homogeneous sub-collections, each of which can be represented by a single atlas image. Specifically, we propose a three-step algorithm. First, we partition the input images into subgroups using unsupervised or semi-supervised learning methods on manifolds. Then we formulate a convex optimization problem in each subgroup to locate the atlases and determine the crucial neighbors that are used in the realization step to form the template images. We have evaluated our algorithm using whole brain MR volumes from OASIS database. Experimental results demonstrate that the atlases computed using the proposed algorithm not only discover the brain structural changes in different age groups but also preserve important structural details and generally enjoy better image quality.

**Index Terms**—Atlas construction, manifolds, optimization, semi-supervised learning.

## I. INTRODUCTION

ATLASES as informative representatives of a population of images have been widely used in many medical imaging applications such as template-based image alignment [1], atlas-based image segmentation [2]–[5], and statistical analysis across subjects [6], [7]. In addition, for heterogeneous or longitudinal data sets, multiple atlases are usually required to provide an informative and complete representation of the image data. For example, the ages of the subjects in Open

Access Series of Imaging Studies (OASIS) database [8] range from 18 to 96. Since the structural difference in the brain across different age groups can be significant [9], it is not appropriate to construct a single representative atlas image for the OASIS data. Not surprisingly, algorithms and methods for computing multiple atlases from image collections have attracted considerable amount of attention recently, and in particular, the unbiased diffeomorphic atlas construction algorithm proposed in [10] has been influential for several notable recent developments such as the iCluster algorithm proposed in [11].

The iCluster algorithm computes multiple atlases by fitting a Gaussian mixture model to the input images using expectation-maximization algorithm (EM) similar in spirit to the unbiased diffeomorphic atlas construction algorithm. A common and visible feature of the atlas images generated by the conventional algorithms ([10], [11]) is their characteristic blurriness and the apparent absence of clear and sharp anatomical details. With their characteristic lack of image fidelity, the computed atlases do not come across as real specimen of MRI images of human brains, a shortcoming that could be critical in some applications. For instance, a clear and sharp atlas is important for the accuracy of atlas-based image registration and segmentation, because it is difficult to find reliable feature correspondences between the sharp input images and a template with blurry and fuzzy structures. In the clinical setting, a clear and sharp atlas image as an informative representative of a sub-population of patients is certainly more meaningful and accessible to medical practitioners than a fuzzy atlas image without clearly identifiable anatomical details.

This loss of image details and structures can be traced back to the atlas construction step (M-step) of the iCluster algorithm in which the atlas is computed as the arithmetic average of group-wise registered images, a popular atlas-construction paradigm first introduced in [10]. It is our observation that the unbiased diffeomorphic atlas construction algorithm often produces blurry and fuzzy atlas images unless the input images are highly homogeneous in their structures. Unfortunately, this is usually not the case and the computed atlases almost always suffer from the loss of image details in various degrees. This undesirable shortcoming can be explained in both practical and theoretical terms. In practice, the existing numerical algorithms used for computing group-wise registration cannot guarantee a globally optimal solution, and unless the images are unusually similar, non-negligible registration errors cannot be avoided in general. Coupled with the suboptimal choices of regularization constants that are often difficult to determine, it is not difficult to imagine a blurry and fuzzy atlas computed as the pixel-wise arithmetic mean of many inaccurately group-wise registered images, which

Manuscript received August 30, 2012; revised December 03, 2012; accepted December 19, 2012. Date of publication January 14, 2013; date of current version February 27, 2013. The work was supported in part by the National Institutes of Health (NIH) under Grant NS066340 to B. C. Vemuri, and in part by the National Science Foundation (NSF) under Grant IIS 0916001 to J. Ho and B. C. Vemuri. *Asterisk indicates corresponding author.*

Y. Xie and J. Ho are with the Department of Computer and Information Science and Engineering (CISE), University of Florida, Gainesville, FL 32611 USA (e-mail: yxie@cise.ufl.edu; jho@cise.ufl.edu).

\*B. C. Vemuri is with the Department of Computer and Information Science and Engineering (CISE), University of Florida, Gainesville, FL 32611 USA (e-mail: vemuri@cise.ufl.edu).

Color versions of one or more of the figures in this paper are available online at <http://ieeexplore.ieee.org>.

Digital Object Identifier 10.1109/TMI.2013.2239654

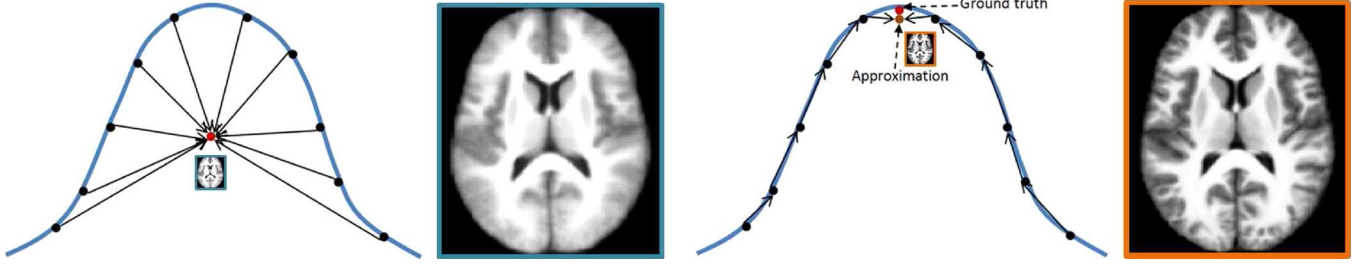


Fig. 1. Ten points on a 1-D manifold. Left: Mean of the ten points computed using the metric of the ambient space (iCluster). Right: Mean computed using the metric of the submanifold  $\mathbf{M}$  (proposed method). Notice the greater preservation of image features and structures in the atlas on the right.

leads to the irreversible loss of structural details. The second and more geometric explanation can be offered as in Fig. 1. The smooth variation of the input images allows us to assume (e.g., [12]) that these images belong to some smooth submanifold  $\mathbf{M}$  in the ambient image space  $\mathcal{I}$ . Unfortunately, this manifold structure is usually difficult to model directly and perhaps more importantly, it is difficult to utilize in the group-wise registration framework. Therefore, in essence, the unbiased diffeomorphic atlas construction algorithm computes the mean of the images in the ambient image space  $\mathcal{I}$ , and as the figure shows, this does not guarantee that the result will be on or near the submanifold  $\mathbf{M}$ . This results in the loss of common image features and renders the atlas images often blurry and fuzzy.

In the context of multiple atlas construction from a large image collection, this paper proposes a novel atlas construction algorithm based on two novel conceptual improvements that aim to correct the shortcomings described above. First, unlike the EM algorithm proposed in [11], we will explicitly decouple the clustering and atlas construction steps. This decoupling provides us with greater flexibility in applying manifold learning methods (e.g., [13], [14]) to model the manifold  $\mathbf{M}$ , an objective that is difficult to accomplish using the traditional EM-based Gaussian mixture model as in [11]. Furthermore, this flexibility also allows us to readily incorporate labeled images in a semi-supervised context, again an objective that would be awkward to formulate using the frameworks proposed earlier (e.g., [10], [11]). Second, we will abandon the usual paradigm of computing the atlas image as the arithmetic mean of all group-wise registered images. Instead, following the manifold assumption, we will propose a new paradigm for atlas image construction by computing the atlas as the weighted arithmetic mean of group-wise registered images. Fig. 1 illustrates the main idea that the mean (atlas) should be mostly determined by its neighbors, and its computation could be formulated in a two-step process that first determines the neighbors of the abstract mean on the manifold  $\mathbf{M}$  (localization) and then renders the mean as an atlas image using these neighbors (realization).

The proposed multiple atlas construction algorithm incorporates the ideas discussed above: A  $k$ -nearest neighbor graph ( $k$ -NN) is used to model the manifold structure of  $\mathbf{M}$  [13], [14], and the graph partition algorithm is applied to the  $k$ -NN graph to compute clusters of the input images. Each atlas is computed as the mean of the images belong to each cluster on  $\mathbf{M}$ . In general, the metric on  $\mathbf{M}$  is unknown; however, the pairwise geodesic distances  $d_{ij} = d_{\mathbf{M}}(\mathbf{I}_i, \mathbf{I}_j)$  between images can be estimated

using the metric in the quotient space  $\mathbf{Q}$ . An important element in the proposed algorithm is to estimate the geodesic distances  $d_{\mathbf{M}}(\bar{\mathbf{I}}, \mathbf{I}_i)$  between the abstract mean  $\bar{\mathbf{I}}$  on  $\mathbf{M}$  and images  $\mathbf{I}_i$  using the pairwise geodesic distances  $d_{ij}$  as the inputs. We formulate this as a convex optimization problem, and the solution to this optimization problem will provide an approximation to  $d_{\mathbf{M}}(\bar{\mathbf{I}}, \mathbf{I}_i)$ . This will allow us to locate the mean  $\bar{\mathbf{I}}$  on the manifold  $\mathbf{M}$  in the localization step by determining its neighbors (given a threshold). In the realization step, we use the weighted group-wise registration method to form the atlas images in each cluster given the estimated neighbors of the atlas. The proposed algorithm has been extensively evaluated and validated using OASIS data, and the experimental results have shown that, with greater preservation of important image features and details, the image atlases produced by the proposed algorithm enjoy better image sharpness and achieve higher segmentation accuracy in label propagation applications when compared with atlases obtained using exiting methods.

## II. MOTIVATION AND RELATED WORK

Image atlas as a standard template has been widely used for the discovery of dense correspondences between MR images of different subjects. Thus, it is natural to construct the image atlas based on group-wise image registration (e.g., [10]). In this type of approach, the atlas formation is cast into an iterative energy minimization framework: input images are nonrigidly registered to a template in the common domain and the template is updated by averaging the aligned images. Unfortunately, because of the large number of variables and the nonconvex cost functional, this algorithm, similar to many others, cannot avoid the prickly traps of local minima. Moreover, the rigidity of the framework makes it difficult to incorporate other useful models and information in the computation.

In recent years, manifold learning techniques have percolated into the medical image analysis community, and they have found successes in several recent works. Gerber *et al.* [15] performed brain population analysis by projecting input brain images onto a low-dimensional space using Isomap [13]. Hamm *et al.* [16] proposed a framework for registering images to the atlas on anatomical manifolds. Their empirical manifold is constructed from input images as a  $k$ -NN graph. A sample from the input population with the smallest sum of squares of geodesic distances to all input images is selected as the atlas. Jia *et al.* [17] introduced a hierarchical groupwise registration framework using the  $k$ -NN Isomap that provides the intrinsic

structure of the input image dataset for their algorithm. However, all the methods discussed above construct a single atlas for the entire input image set, which implicitly assumes a homogeneous population, an assumption that is inappropriate for studying heterogeneous image data sets that are far more common and important in medical imaging analysis. iCluster is an EM-based algorithm presented by [18] for computing multiple template images for an image population. The algorithm fits a Gaussian mixture model to the input images and the input images are not assumed to possess an intrinsic manifold structure. Furthermore, it is well known that the optimization in the EM-algorithm cannot guarantee the globally optimal solution, and therefore, good initializations of the EM-algorithm, which may not be available or even possible, are critical for the success of the method.

In this paper, we extend our previous work [19] to the multiple atlas construction problem. Several pertinent features distinguish our method from the iCluster [18] and many previously published methods. First, we use the quotient space  $\mathbf{Q}$  of the image space  $\mathcal{I}$  by the rotation group as the ambient image space instead of the usual image space  $\mathcal{I}$  itself. Intuitively, a brain image  $\mathbf{I}$  and its rotated version  $\mathbf{I}'$  both represent the same subject. Thus a rotational invariant distance needs to be introduced such that the distance between  $\mathbf{I}$  and  $\mathbf{I}'$  is zero. Modeling the objects invariant to some group actions has been an important research topic in computer vision and medical image analysis for more than a decade. In [20], Miller and Younes introduced image metrics defined between orbits under group actions and successfully applied them to image matching. Kurtek *et al.* utilized q-map which is invariant under both rotation and re-parametrization groups in the shape analysis of multiple brain structures [21]. In our work, we employ a similar approach by utilizing the metric between rotation orbits in  $\mathcal{I}$  to define the distance in the quotient space  $\mathbf{Q}$ . Second, the proposed method explicitly models the intrinsic manifold structure in the quotient space  $\mathbf{Q}$  using manifold learning ( $k$ -NN graph) [13], [14], [22]. As illustrated in Fig. 1, the image data set usually has the special structure which needs to be incorporated in the atlas construction. Moreover, we explicitly identify two important steps in the atlas formation process: localization and realization. We formulate a convex cost function in the localization step that bypasses the difficulty of globally minimizing the complicated nonconvex functional, and in the realization step, we perform the weighted group-wise registration such that only a few subjects close to the mean have high weights, while the faraway subjects have very low weights in generating the atlas image. A similar idea is also presented in the recent work SharpMean [23] in which, Wu *et al.* developed an adaptively weighted strategy to compute the sharp group mean image which is a weighted average of the aligned subjects. Different from our method, the median image of the input subjects under Euclidean distance was chosen as the initial template and the weight of each subject for generating the group mean image was also different across the spatial locations.

### III. METHODS

The primary aim of our algorithm is to produce rotationally-invariant atlas images that retain clear important anatomical

structures common to the subpopulation of images they represent. The strategy for achieving these two somewhat disparate goals is to utilize the notion of manifold structure implied by the images. Specifically, we will assume, as in many manifold-based learning methods (e.g., [24], [25]), that the input images are samples from an unknown manifold  $\mathbf{M}$ , and the manifold structure is then modeled using a graph  $G$  computed from the input images and some metric (e.g., similarity) information among the images. The rotational invariance requirement implies that the manifold of interest  $\mathbf{M}$  should be considered as a submanifold of a quotient space (quotient by the rotations), and computationally, this requires rotationally-invariant metric for computing the graph  $G$ . The graph  $G$  allows us to partition the image collection into subcollections, in both supervised and semi-supervised fashion, such that an atlas can be computed from each subcollection of images using only metrical information between the images.

#### A. Rotational Invariance and the Geometry of the Quotient Space $\mathbf{Q}$

Let  $\mathcal{I}$  denote the space of images, and we define images in  $\mathcal{I}$  formally as  $L^2$ -functions on a finite image domain  $\Omega \subset \mathbb{R}^d$  ( $d = 2$  for 2-D images and  $d = 3$  for 3-D images). Let  $\mathcal{C} \equiv \{\mathbf{I}_1, \dots, \mathbf{I}_n\}$  denote an input collection of  $n$  images and  $\mathcal{A} \equiv \{\mathbf{I}_{a_1}, \dots, \mathbf{I}_{a_t}\}$  the collection of  $t$  atlases for the image collection  $\mathcal{C}$ . A rotation  $g \in \mathbf{SO}(d)$  in the image domain  $\Omega$  transforms an image  $\mathbf{I}$  into a rotated image  $g(\mathbf{I})$  according to the formula  $g(\mathbf{I})(x) = \mathbf{I}(g^{-1}(x))$  for  $x \in \Omega$  and  $\mathbf{I} \in \mathcal{I}$ . Let  $\mathcal{C}' \equiv \{\mathbf{I}'_1, \dots, \mathbf{I}'_n\}$  denote the images obtained by applying  $n$  rotations to images in  $\mathcal{C}$ :  $\mathbf{I}'_i = g_i(\mathbf{I}_i)$  for  $g_i \in \mathbf{SO}(d)$ ,  $1 \leq i \leq n$ , the atlases  $\mathcal{A}' \equiv \{\mathbf{I}'_{a_1}, \dots, \mathbf{I}'_{a_t}\}$  computed for  $\mathcal{C}'$  are different from the atlases in  $\mathcal{A}$  up to rotations, i.e.,  $\mathbf{I}'_{a_j} = r_j(\mathbf{I}_{a_j})$  for  $r_j \in \mathbf{SO}(d)$ ,  $1 \leq j \leq t$ . The rotational invariance property requires us to work not in the image space  $\mathcal{I}$  but in its quotient space  $\mathbf{Q}$ , the quotient space of  $\mathcal{I}$  by the rotation group  $\mathbf{SO}(d)$  [26], [27]. The quotient space  $\mathbf{Q}$  is a space that parameterizes the  $\mathbf{SO}(d)$ -orbits in  $\mathcal{I}$  and in this paper, we will assume that  $\mathbf{Q}$  has a manifold structure induced from the manifold structure of  $\mathcal{I}$ . Let  $\pi : \mathcal{I} \rightarrow \mathbf{Q}$  denote the canonical projection map that sends each image  $\mathbf{I} \in \mathcal{I}$  to the unique  $\mathbf{SO}(d)$ -orbit  $[\mathbf{I}] \in \mathbf{Q}$  containing  $\mathbf{I}$ :  $\pi(\mathbf{I}) = [\mathbf{I}]$ .

There is a well-known bijective correspondence [27] between metrics on  $\mathbf{Q}$  and  $\mathbf{SO}(d)$ -invariant metric on  $\mathcal{I}$ . Recall that a  $\mathbf{SO}(d)$ -invariant metric on  $\mathcal{I}$  satisfies the following condition:

$$d_{\mathcal{I}}(\mathbf{I}_1, \mathbf{I}_2) = d_{\mathcal{I}}(g(\mathbf{I}_1), g(\mathbf{I}_2))$$

for any two images  $\mathbf{I}_1, \mathbf{I}_2 \in \mathcal{I}$  and  $g \in \mathbf{SO}(d)$ . The correspondence between metrics  $d_{\mathbf{Q}}$  on  $\mathbf{Q}$  and  $\mathbf{SO}(d)$ -invariant metrics  $d_{\mathcal{I}}(x, y)$  on  $\mathcal{I}$  is provided by the formula [27]

$$d_{\mathbf{Q}}([\mathbf{I}_1], [\mathbf{I}_2]) = \min_{x \in [\mathbf{I}_1], y \in [\mathbf{I}_2]} d_{\mathcal{I}}(x, y) \quad (1)$$

for any two points  $[\mathbf{I}_1], [\mathbf{I}_2] \in \mathbf{Q}$ . Note that  $[\mathbf{I}_1], [\mathbf{I}_2]$  are realized in  $\mathcal{I}$  as  $\mathbf{SO}(d)$ -orbits, and  $d_{\mathbf{Q}}$  simply computes the distance between the two orbits in  $\mathcal{I}$  as measured by  $d_{\mathcal{I}}$  in  $\mathcal{I}$ . Because of the property of  $\mathbf{SO}(d)$ -invariant metrics,  $d_{\mathbf{Q}}$  can be computed

with respect to only one transformation instead of a rotation per each orbit

$$\mathbf{d}_{\mathbf{Q}}([\mathbf{I}_1], [\mathbf{I}_2]) = \min_{g \in \mathbf{SO}(d)} \mathbf{d}_{\mathcal{I}}(g(\mathbf{I}_1), \mathbf{I}_2). \quad (2)$$

The two related metrics  $\mathbf{d}_{\mathcal{I}}$ ,  $\mathbf{d}_{\mathbf{Q}}$  allows us to go between  $\mathcal{I}$  and  $\mathbf{Q}$ . In particular, any computation relating to a metric on  $\mathbf{Q}$  can be equivalently formulated using its corresponding  $\mathbf{SO}(d)$ -invariant metric on  $\mathcal{I}$ . Fortunately, many metrics in  $\mathcal{I}$  can be easily shown to be  $\mathbf{SO}(d)$ -invariant, such as the usual  $L^2$ -metric and the following metric proposed in [12]:

$$\mathbf{d}_{\mathcal{I}}(\mathbf{I}_1, \mathbf{I}_2) = \min_{h_i} \left( \int_{\Omega} |\mathbf{I}_1(h_i(x)) - \mathbf{I}_2|^2 dx + \int_0^1 \int_{\Omega} \|Lv_i\|^2 dx ds \right)^{1/2} \quad (3)$$

where  $v_i$  is the time-dependent vector field that defines the diffeomorphic flow from the identity to the diffeomorphism  $h_i$ , and  $L$  is a second-order elliptic operator. The metric in (3) can be computed by using nonrigid diffeomorphic image registration. Given the images  $\mathbf{I}_i$  in  $\mathcal{C}$ , the manifold  $\mathbf{M}$  that will be modeled pertains to the points  $\{[\mathbf{I}_1], \dots, [\mathbf{I}_n]\}$  in the quotient space  $\mathbf{Q}$ . As a submanifold of  $\mathbf{Q}$ ,  $\mathbf{M}$  is naturally equipped with the induced Riemannian metric, and in the following, we will denote  $\mathbf{d}_{\mathbf{M}}([\mathbf{I}_i], [\mathbf{I}_j])$  the geodesic distance function on  $\mathbf{M}$ .

### B. Graph Representation of the Manifold $\mathbf{M}$

Because the manifold  $\mathbf{M}$  does not have explicit representation, we follow the common approach that uses a graph  $G = (V, E)$  to characterize its manifold structure, where  $V, E$  are the node and edge sets, respectively. In this construction, the node set  $V = \{[\mathbf{I}_1], \dots, [\mathbf{I}_n]\}$  is provided by the points  $[\mathbf{I}_i]$  in the quotient space  $\mathbf{Q}$ . The edge set  $E$  that defines the connectivity of  $G$  is determined by the pair-wise distances among the points  $[\mathbf{I}_i]$  via the standard  $k$ -nearest neighbor ( $k$ -NN) construction. That is, an edge is formed between every node and its  $k$  nearest neighbors.

Because of the heterogeneity of some image sets, we partition the graph  $G$  into  $t$  subgraphs in order to compute multiple atlases to represent the image sets. Spectral clustering and related methods provide a readily available algorithms for partitioning the graph  $G$ . Popular and well-known algorithms include Ratio Cut [28] and Normalized Cut [29]. The algorithm partitions the graph using the graph Laplacian matrix  $\mathbf{L}$  that is computed from the similarity matrix  $\mathbf{W}$  that encodes all the metrical information provided by the nodes  $[\mathbf{I}_i]$

$$W_{ij} = \begin{cases} \exp\left(-\frac{\mathbf{d}_{\mathbf{Q}}([\mathbf{I}_i], [\mathbf{I}_j])^2}{\sigma^2}\right), & \text{if } j \in \mathcal{N}_i \text{ or } i \in \mathcal{N}_j \\ 0, & \text{otherwise} \end{cases} \quad (4)$$

where  $\mathcal{N}_i$  and  $\mathcal{N}_j$  are  $k$  nearest neighborhoods. The parameter  $\sigma$  is empirically estimated by  $\sigma = (1/n) \sum_{i=1}^n \mathbf{d}_{\mathbf{Q}}([\mathbf{I}_i], [\mathbf{I}_{i_k}])$  where  $[\mathbf{I}_{i_k}]$  is the  $k$ th nearest neighbor of  $[\mathbf{I}_i]$ . The graph Laplacian matrix is defined as

$$\mathbf{L} = \mathbf{D} - \mathbf{W} \quad (5)$$

where  $\mathbf{D}$  is an  $n \times n$  diagonal matrix with  $D_{ii} = \sum_{j=1}^n W_{ij}$ . After the partition, we obtain  $t$  subgraphs  $G_i = (V_i, E_i)$ , where  $V_1, \dots, V_t$  is the partition of the set  $V$  and  $E_i \subset E$  only includes edges whose two vertices are in  $V_i$ .

The above unsupervised framework can be easily extended to a semi-supervised framework with partially labeled data. Inspired by the ideas from semi-supervised learning [24], [25], we consider the graph partition problem with partially labeled nodes as a classification problem that transfers the known labels to the unlabeled data.

We will first consider the two-class partition problem with the label set  $Y = \{-1, 1\}$ . It can be formulated as a binary classification problem on the manifold with the classifier defined as a function:  $f : \mathbf{M} \rightarrow Y$ . When  $\mathbf{M}$  is a compact manifold, the eigenfunctions of the Laplace–Beltrami operator  $\Delta$  provide a natural orthogonal basis for the Hilbert space  $L^2(\mathbf{M})$  [25], i.e., any function  $f \in L^2(\mathbf{M})$  can be written in terms of the eigenfunctions of  $\Delta$

$$f(x) = \sum_{i=1}^{\infty} a_i u_i(x) \quad (6)$$

where  $a_i$  are coefficients and  $u_i$  are eigenfunctions such that  $\Delta u_i = \lambda_i u_i$ . Thus we could fit the classifier on the labeled data and find the optimal model parameters  $\mathbf{a}$  which will be used to classify the unlabeled data. Let the sample set be  $\mathcal{X} = \{x_1, \dots, x_s, x_{s+1}, \dots, x_n\} \subset \mathbf{M}$ . Without loss of generality, we assume the first  $s$  data  $\{c_1, \dots, c_s\}$ ,  $c_i \in Y$  are labeled and others are unlabeled. Given the graph Laplacian  $\mathbf{L}$ , we can solve the eigenvector problem  $\mathbf{L}\mathbf{u} = \lambda\mathbf{u}$  to generate the corresponding eigenfunctions. Let  $\mathbf{u}_1, \dots, \mathbf{u}_p$  be eigenvectors corresponding to the  $p$  smallest eigenvalues.  $\mathbf{u}_i = [u_{i1}, \dots, u_{in}]^T$ , where  $i = 1, \dots, p$ . Then the classifier is trained from the labeled data by minimizing the cost function

$$\mathcal{E}(\mathbf{a}) = \sum_{i=1}^s \left( c_i - \sum_{j=1}^p a_j u_{ji} \right)^2 = \|\mathbf{U}\mathbf{a} - \mathbf{c}\|^2 \quad (7)$$

where the coefficients  $\mathbf{a} = [a_1, \dots, a_p]^T$ , the labels  $\mathbf{c} = [c_1, \dots, c_s]^T$  and the basis matrix  $\mathbf{U} = \begin{pmatrix} u_{11} & \dots & u_{p1} \\ \vdots & \ddots & \vdots \\ u_{1s} & \dots & u_{ps} \end{pmatrix}$ .

The closed-form solution of this optimization problem is  $\mathbf{a} = (\mathbf{U}^T \mathbf{U})^{-1} \mathbf{U}^T \mathbf{c}$ . For the unlabeled data  $x_i$ ,  $i > s$ , we just apply the trained classifier and set the label to be 1 if  $\sum_{j=1}^p a_j u_{ji} \geq 0$ , otherwise the label is set to  $-1$ . For  $t$ -classes graph partition,  $t > 2$ , we follow the *one-versus-the-rest* approach that is commonly used in multiclass support vector machines [30]. We build  $t$  separate two-class classifiers  $f_k$ , where  $k = 1, \dots, t$ . The  $k$ th classifier is estimated by using the data from class- $k$  as the positive samples and the data from remaining  $t - 1$  classes as the negative samples. Then  $t$  coefficients  $\mathbf{a}_k = [a_{k1}, \dots, a_{kp}]^T$ ,  $1 \leq k \leq t$  are computed and will be used to classify unlabeled data. For  $x_i$ ,  $i > s$ , the label is set to be  $\arg \max_k f_k(x_i) = \sum_{j=1}^p a_{kj} u_{ji}$ . This multi-class

semi-supervised graph partition algorithm is summarized in Algorithm 1.

**Algorithm 1** Semi-supervised graph partition

- 1: Compute similarity matrix  $\mathbf{W}$  and graph Laplacian matrix  $\mathbf{L}$  using both labeled and unlabeled data.
- 2: Solve the eigenvector problem,  $\mathbf{L}\mathbf{u} = \lambda\mathbf{u}$ . Let  $\mathbf{u}_1, \dots, \mathbf{u}_p$  be  $p$  eigenvectors corresponding to the  $p$  smallest eigenvalues.
- 3: Give  $s$  labeled data, we will train  $t$  separate two-class classifiers. To estimate the  $k$ th classifier  $f_k$ ,  $1 \leq k \leq t$ , we first form a label set  $\mathbf{c}_k$  such that the data in class- $k$  have the label value 1 and the data in remaining classes have the label value  $-1$ . Then we minimize the following cost function:
 
$$\mathcal{E}(\mathbf{a}_k) = \|\mathbf{U}\mathbf{a}_k - \mathbf{c}_k\|^2 \quad (8)$$
 and obtain the coefficients  $\mathbf{a}_k = (\mathbf{U}^T\mathbf{U})^{-1}\mathbf{U}^T\mathbf{c}_k$  in the linear classifier  $f_k$ .
- 4: We use the coefficients  $\mathbf{a}_k = [a_{k1}, \dots, a_{kp}]^T$ ,  $1 \leq k \leq t$  computed from step 3 to classify the unlabeled data. For  $x_i$ ,  $i > s$ , the label is simply set as  $\arg \max_k \sum_{j=1}^p a_{kj}u_{ji}$ .

*C. Estimating Mean From Pairwise Geodesic Distances*

After the graph partition, we need to construct an atlas for each subgraph. Without loss of generality, we suppose  $\{x_1, \dots, x_n\}$  are nodes of one subgraph  $G_a$  on a manifold  $\mathbf{M}$ . Let  $\bar{x} \in \mathbf{M}$  denote the mean of points  $\{x_1, \dots, x_n\}$  on  $\mathbf{M}$  and  $\mathbf{d}_\mathbf{M}$  denotes the Riemannian geodesic distance on  $\mathbf{M}$ . Although we do not have the analytic representation for  $\mathbf{d}_\mathbf{M}$ , we could approximate  $\mathbf{d}_\mathbf{M}(x_i, x_j)$ ,  $1 \leq i, j \leq n$  with  $\mathbf{d}_\mathbf{Q}$  and the graph structure of  $G_a$ . For each edge  $(x_p, x_q) \in E_a$ , let the distance  $\mathbf{d}_\mathbf{Q}(x_p, x_q)$  be its weight. Because a geodesic is defined as the shortest path between two points on the manifold, inspired by the approach in ISOMAP [13], we could use Dijkstra's algorithm or the Floyd-Warshall algorithm [31] to find the shortest path between two nodes  $x_i, x_j$  on the graph and use it to approximate the geodesic on the manifold  $\mathbf{M}$ . One possible way to determine the mean  $\bar{x}$  is the following. Let  $a_i = \mathbf{d}_\mathbf{M}(x_i, \bar{x})$ ,  $1 \leq i \leq n$ . Determining  $a_i$  is of course equivalent to locating  $\bar{x}$  on  $\mathbf{M}$ , and  $a_i$  can be determined as the solution to an optimization problem given by

$$\begin{aligned} \min \quad & a_1^2 + a_2^2 + \dots + a_n^2 \\ \text{s.t.} \quad & a_i \geq 0, \quad i = 1, \dots, n \\ & a_i + a_j \geq \mathbf{d}_\mathbf{M}(x_i, x_j) \\ & a_i + \mathbf{d}_\mathbf{M}(x_i, x_j) \geq a_j \\ & a_j + \mathbf{d}_\mathbf{M}(x_i, x_j) \geq a_i, \quad j = 1, \dots, n. \end{aligned} \quad (9)$$

The linear inequality constraints between  $a_i$  and  $\mathbf{d}_\mathbf{M}(x_i, x_j)$  are imposed because  $\mathbf{d}_\mathbf{M}$  satisfies the triangle inequality [32]. For our problem, the manifold  $\mathbf{M}$  and its metric  $\mathbf{d}_\mathbf{M}$  are unknown, and consequently, the higher-degree constraints cannot be known. Thus, only linear constraints are considered in this paper.

The optimization problem is clearly convex since the objective function is strictly convex (the Hessian is positive-definite everywhere) and the domain, which is the intersection of half-spaces, is also convex. This particular type of optimization problem (with quadratic cost function and linear inequality constraints) can be solved efficiently even with a large number of variables and constraints. And because the objective function is strictly convex, the solution is unique [33]. Furthermore, the solution is stable with respect to the input parameters  $\mathbf{d}_\mathbf{M}(x_i, x_j)$  in the sense that small perturbations of  $\mathbf{d}_\mathbf{M}(x_i, x_j)$  will not significantly alter the solution  $a_1, \dots, a_n$  [33]. The quadratic programming problem in (9) is special in that the Hessian in the objective function is just a diagonal matrix and the constraint matrix is sparse. Therefore, in our experiments, we choose the interior point method which can handle large-scale quadratic optimization problem. For computing robust  $\mathbf{L}^1$ -median [34] instead of mean, we simply need to change the cost function to  $a_1 + a_2 + \dots + a_n$ .

*D. Computing the Image Atlases*

The result of the previous localization step provides us with the pairwise distances  $\mathbf{d}_\mathbf{M}(\bar{\mathbf{I}}, [\mathbf{I}_i])$ , and at this point, the atlas has been located only in the abstract manifold  $\mathbf{M}$  in terms of these distances. In the realization step, we will render the atlas image using the distance data  $\mathbf{d}_\mathbf{M}(\bar{\mathbf{I}}, [\mathbf{I}_i])$  and the input images. Specifically, given the vertex set  $\{[\mathbf{I}_1], \dots, [\mathbf{I}_n]\}$  of subgraph  $G_a$  and the corresponding non-negative numbers  $a_i$  as estimates on the geodesic distances  $\mathbf{d}_\mathbf{M}(\bar{\mathbf{I}}, [\mathbf{I}_i])$ , where  $i = 1, \dots, n$ , we realize the image atlas using a weighted group-wise registration approach. Because the closer a sample image to the atlas on the manifold  $\mathbf{M}$ , the more contribution it will give in atlas realization, the weight is in the form of an exponential function  $\exp(-a_i^2/\sigma^2)$ . Given the  $k$ -NN graph,  $\sigma$  is empirically estimated by the  $k$ th smallest  $a_i$ . Since the weight will be close to 0 if  $a_i$  is large, we determine  $K$  points in  $\{[\mathbf{I}_1], \dots, [\mathbf{I}_n]\}$  that are close to  $\bar{\mathbf{I}}$  as measured by  $\mathbf{d}_\mathbf{M}$ , and the atlas image is then approximated from these points with respect to the metric  $\mathbf{d}_\mathbf{Q}$  in  $\mathbf{Q}$ . In practice, a positive integer  $K$  is specified such that the sum of weights of  $K$  points  $[\mathbf{I}_{i_1}], \dots, [\mathbf{I}_{i_K}]$  with shortest distances to  $\bar{\mathbf{I}}$  covers more than 95% of the total weight.

We approximate  $\bar{\mathbf{I}}$  by solving the following optimization problem:

$$\bar{\mathbf{I}} = \underset{[\mathbf{I}'] \in \mathbf{Q}}{\operatorname{argmin}} \sum_{j=1}^K w_j \mathbf{d}_\mathbf{Q}^2([\mathbf{I}_{i_j}], [\mathbf{I}']) \quad (10)$$

where  $w_j$  is determined by the estimated geodesic distances  $a_{i_j}$

$$w_j = \frac{b_j}{\sum_{k=1}^K b_k}$$

with  $b_j = \exp(-a_{i_j}^2/\sigma^2)$ ,  $1 \leq j \leq K$ . Using the metric defined by (3), the corresponding atlas  $\bar{\mathbf{I}}$  is computed by solving the variational problem

$$\min_{\bar{\mathbf{I}}, h_j, g_j} \sum_{j=1}^K w_j \left( \int_{\Omega} |\mathbf{I}_{i_j}(h_j g_j(x)) - \bar{\mathbf{I}}|^2 dx + \int_0^1 \int_{\Omega} \|L v_j\|^2 dx ds \right)$$

where  $L$  is a second-order elliptic operator.

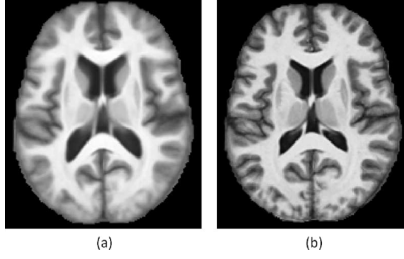


Fig. 2. Axial view of constructed image atlases. Atlases generated using (a) ANTS and (b) the proposed method, respectively.

#### IV. EXPERIMENTS

In this section, we apply the proposed algorithms to compute atlases from collections of MR images and compare with the conventional image atlas construction methods ANTS [35] and iCluster [11], [18]. Specifically, the image data used in our experiment are the MR images from the freely available Open Access Series of Imaging Studies (OASIS) dataset [8]. OASIS contains T1 weighted MR brain images from a cross-sectional population of 416 subjects. Each MR scan has the size of  $176 \times 208 \times 176$  voxels and the resolution of  $1 \times 1 \times 1$  mm<sup>3</sup>. The ages of the subjects range from 18 to 96. For each subject, a labeled image with segmentations of white matter (WM), gray matter (GM), and cerebrospinal fluid (CSF) is also provided.

##### A. Single Atlas for OASIS Data

In the first experiment, we evaluated the performance of our graph-based single atlas construction method. For comparison, we employed the image template construction method provided by Advanced Normalization Tools (ANTS), which is a state-of-the-art ITK-based toolkit for computational anatomy. We used symmetric diffeomorphic transformation and the mean squared similarity measure in our experiment. Fifty subjects across different ages were selected from the OASIS dataset for the atlas construction. The image atlases constructed by the proposed method and ANTS are shown in Fig. 2. It is clear that our sharp image template preserves better the subtle anatomical structures than the fuzzy mean image generated by the conventional atlas construction method in ANTS.

In order to quantitatively evaluate the effectiveness of the proposed atlas construction method, we also conducted an experiment on atlas-based image segmentation. Since the deformation of each input image to the atlas is computed, the corresponding WM/GM/CSF label map can be warped to the reference domain. We set the tissue label of the image atlas at each voxel as the majority of tissue assignments from all registered images. Then the image template with the tissue label map was warped to 10 additional OASIS subjects to achieve the atlas-based tissue segmentation. We used the DICE score to quantitatively measure the segmentation accuracy. The segmentation DICE scores of WM, GM, and CSF for the ten OASIS subjects are displayed in Fig. 3. In this atlas-based segmentation application, the image atlas constructed by the proposed method consistently achieves better segmentation accuracy than the mean image template generated by ANTS, with the overall average DICE score 0.7769 by our method and 0.7420 by ANTS.

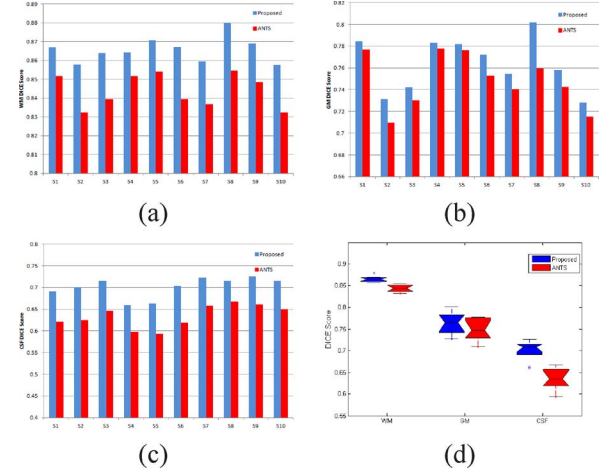


Fig. 3. DICE scores for the segmentation of (a) white matter (WM), (b) gray matter (GM), and (c) cerebrospinal fluid (CSF) for 10 subjects in OASIS. (d) Box plot of the segmentation results.

TABLE I  
MEANS AND STANDARD DEVIATIONS OF SUBJECT AGES  
FOR THE TWO CLASS PARTITION

	iCluster	unsupervised	semi-supervised	selected
Class 1	$39.1 \pm 19.9$	$37.3 \pm 18.7$	$33.7 \pm 17.0$	$27.7 \pm 9.9$
Class 2	$77.8 \pm 9.3$	$77.0 \pm 9.9$	$75.3 \pm 9.6$	$73.7 \pm 10.3$

##### B. Multiple Atlases for OASIS Data

Because the structural difference in the brain across different age groups can be significant [9], the OASIS data set is far from homogeneous. Therefore, instead of a single mean template image, multiple atlases are required to represent the whole OASIS data satisfactorily. In the first part of this experiment, we constructed two atlases for the collection of 416 subjects in the OASIS dataset using both the unsupervised and semi-supervised methods. In all following experiments, we set  $k = 10$  when constructing the k-NN graphs. For the unsupervised graph partition, we use two clusters, and for the semi-supervised graph partition, we randomly choose 20 subjects younger than 50 years old and 20 subjects older than or equal to 50 as the labeled samples. The remaining subjects are considered as unlabeled samples. Table I compares the means and standard deviations of ages of subjects in the two clusters computed by EM-based iCluster algorithm [18], our unsupervised and semi-supervised methods. The means and standard deviations of two age groups separated by 50 are also listed in Table I as a reference. The clustering result of our unsupervised method is similar to iCluster, while our semi-supervised method gives slightly smaller mean ages for both young and old groups.

The partial labels in semi-supervised learning provide useful information to correctly classify more subjects aged between 50 and 70 into the older group. As shown in Fig. 4, the atlases generated by iCluster are blurry, while the atlases computed by our methods are substantially sharper, retaining more structural details. The age histogram also reveals that a third cluster for middle-aged subjects can be defined for the OASIS cross-sectional set. Accordingly, in the second experiment, we used



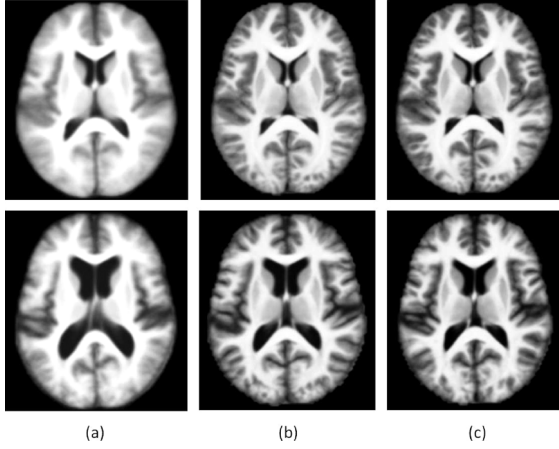


Fig. 4. Two atlases for the OASIS data. Atlases for first row: young subjects; second row: older subjects, respectively. Atlases using (a) iCluster, (b) our unsupervised algorithm, and (c) our semi-supervised algorithm, respectively.

TABLE II  
MEANS AND STANDARD DEVIATIONS OF SUBJECT AGES FOR  
THE THREE CLASS PARTITION

	iCluster	unsupervised	semi-supervised	selected
Class 1	$31.2 \pm 14.5$	$30.3 \pm 13.9$	$30.0 \pm 16.9$	$23.4 \pm 4.4$
Class 2	$68.9 \pm 13.6$	$67.1 \pm 15.2$	$54.6 \pm 14.9$	$50.4 \pm 5.5$
Class 3	$79.6 \pm 7.5$	$79.6 \pm 7.3$	$77.1 \pm 8.5$	$76.5 \pm 8.0$

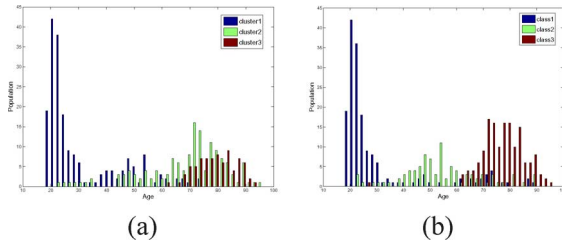


Fig. 5. Three class partition case. (a) Unsupervised method. (b) Semi-supervised method. Figure is best viewed in color.

three clusters for our unsupervised atlases construction algorithm. For the semi-supervised algorithm, we first divided the OASIS population into three groups: young (subjects younger than 40), middle-aged (between 40 and 60), and older adults (older than 60). The means and standard deviations of ages of subjects in these three predetermined groups are displayed in Table II. Then we randomly sampled 20 subjects from each group as the labeled data and considered the remainder unlabeled. The histograms of both unsupervised and semi-supervised partition results are shown in Fig. 5. For our unsupervised method, the middle-aged cluster has a significant overlap with the old cluster, and a similar result was also reported in [18]. The clustering methods employed by both algorithms are designed to detect and discover the dominant structural modes, and there is an obvious structural difference between old (around 60) and elderly (around 75) subjects. This complicates the task of determining the middle-age mode in the age distribution using these clustering techniques. However, since the semi-supervised method uses more information from

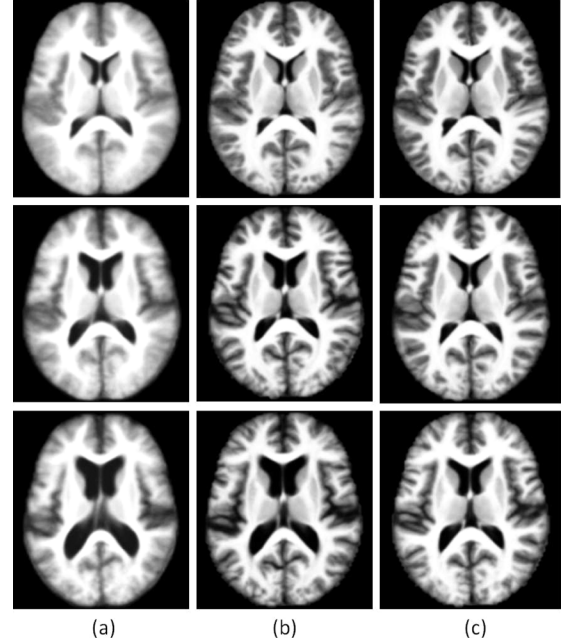


Fig. 6. Three atlases for OASIS data. Atlases for first row: young, second row: middle aged and third row: elderly subjects, respectively. Atlases using (a) iCluster, (b) our unsupervised algorithm, (c) our semi-supervised algorithm, respectively.

partially labeled data, it gives a better classification for different modes in the age distribution. Table II compares the means and standard deviations of ages of subjects in all three classes computed by iCluster, our unsupervised and semi-supervised methods, and Fig. 6 shows the corresponding atlases constructed by these three algorithms. The clustering result of our unsupervised method is similar to iCluster, but our method provides considerably sharper atlases, which are very useful in applications such as atlas-based segmentation and tensor-based morphometry. Compared with corresponding mean ages computed by iCluster and our unsupervised methods, the mean age of class two computed by our semi-supervised partition method is 54.6, which is substantially closer to the mode for the middle-aged group one would expect from the histogram of the age distribution.

With the age information for some subjects, our semi-supervised method has the ability to construct more than three atlases across ages, which is akin to the population shape regression [12]. The regression method requires ages of all subjects in the data set, while our method only needs class labels for a small number of images. The OASIS data can be partitioned into seven classes with ten-year intervals. We randomly chose ten subjects from each class as the labeled data and consider the remaining unlabeled. Note that only 16.8% of images are labeled. The atlases computed across seven different age groups in the OASIS data are shown in Fig. 7. All atlases are sharp with many clearly visible structural details, and in particular, the progressive enlargement of the ventricle with aging can be observed clearly in the atlas sequence and the accelerated expansion of the ventricle after age 60 shown in the atlas sequence corroborates with the findings reported in [9] and [12].

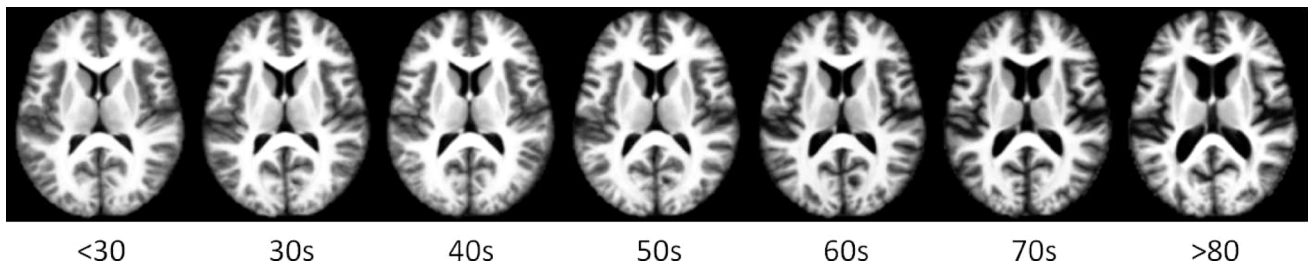


Fig. 7. Atlases across different ages for subjects in the OASIS data set.

## V. CONCLUSION

We have proposed a novel approach to the multiple atlas construction problem that places strong emphasis on capturing structural image details common among the input images. For large image collections with substantial structural heterogeneity, the proposed two-step algorithm first partitions the image collection into (relatively more) homogeneous subcollections followed by a novel atlas construction algorithm that explicitly computes a single image atlas for each subcollection of images. Comparisons with existing methods have shown that the atlases computed using the proposed algorithm capture image sharpness and features to a higher degree.

## REFERENCES

- [1] J. Talairach and P. Tournoux, *Co-Planar Stereotaxic Atlas of the Human Brain*. New York: Thieme, 1988, vol. 147.
- [2] B. Vemuri, J. Ye, Y. Chen, and C. Leonard, "Image registration via level-set motion: Applications to atlas-based segmentation," *Med. Image Anal.*, vol. 7, no. 1, pp. 1–20, 2003.
- [3] B. Fischl *et al.*, "Whole brain segmentation: Automated labeling of neuroanatomical structures in the human brain," *Neuron*, vol. 33, no. 3, pp. 341–355, 2002.
- [4] P. Bazin and D. Pham, "Statistical and topological atlas based brain image segmentation," in *Proc. MICCAI*, 2007, pp. 94–101.
- [5] B. T. Yeo, M. Sabuncu, R. Desikan, B. Fischl, and P. Golland, "Effects of registration regularization and atlas sharpness on segmentation accuracy," *Med. Image Anal.*, vol. 12, no. 5, pp. 603–615, 2008.
- [6] J. Ashburner, C. Hutton, R. Frackowiak, I. Johnsrude, C. Price, and K. Friston, "Identifying global anatomical differences: Deformation-based morphometry," *Human Brain Mapp.*, vol. 6, no. 5–6, pp. 348–357, 1998.
- [7] X. Hua *et al.*, "Tensor-based morphometry as a neuroimaging biomarker for Alzheimer's disease: An MRI study of 676 AD, MCI, and normal subjects," *Neuroimage*, vol. 43, no. 3, pp. 458–469, 2008.
- [8] D. Marcus, T. Wang, J. Parker, J. Gsernansky, J. Morris, and R. Buckner, "Open access series of imaging studies (OASIS): Cross-section MRI data in young, middle aged, nondemented, and demented older adults," *J. Cognitive Neurosci.*, vol. 19, pp. 1498–1507, 2007.
- [9] B. Mortamet, D. Zeng, G. Gerig, M. Prastawa, and E. Bullitt, "Effects of healthy aging measured by intracranial compartment volumes using a designed MR brain database," in *Proc. MICCAI*, 2005, pp. 383–391.
- [10] S. Joshi, B. Davis, M. Jomier, and G. Gerig, "Unbiased diffeomorphic atlas construction for computational anatomy," *NeuroImage*, vol. 23, pp. S151–S160, 2004.
- [11] M. Sabuncu, S. Balci, and P. Golland, "Discovering modes of an image population through mixture modeling," in *Proc. MICCAI*, 2008, pp. 381–389.
- [12] B. Davis, P. Fletcher, E. Bullitt, and S. Joshi, "Population shape regression from random design data," in *Proc. ICCV*, 2007, pp. 1–7.
- [13] J. Tenenbaum, V. de Silva, and J. Langford, "A global geometric framework for nonlinear dimensionality reduction," *Science*, vol. 290, no. 5500, pp. 2319–2323, 2000.
- [14] M. Belkin and P. Niyogi, "Laplacian eigenmaps and spectral techniques for embedding and clustering," *NIPS*, vol. 1, pp. 585–592, 2002.
- [15] S. Gerber, T. Tasdizen, P. Thomas Fletcher, S. Joshi, and R. Whitaker, "Manifold modeling for brain population analysis," *Med. Image Anal.*, vol. 14, no. 5, pp. 643–653, 2010.
- [16] J. Hamm, D. Ye, R. Verma, and C. Davatzikos, "GRAM: A framework for geodesic registration on anatomical manifolds," *Med. Image Anal.*, vol. 14, no. 5, pp. 633–642, 2010.
- [17] H. Jia, G. Wu, Q. Wang, and D. Shen, "ABSORB: Atlas building by self-organized registration and bundling," *NeuroImage*, vol. 51, no. 3, pp. 1057–1070, 2010.
- [18] M. Sabuncu, S. Balci, M. Shenton, and P. Golland, "Image-driven population analysis through mixture modeling," *IEEE Trans. Med. Imag.*, vol. 28, no. 9, pp. 1473–1487, Sep. 2009.
- [19] Y. Xie, J. Ho, and B. Vemuri, "Image atlas construction via intrinsic averaging on the manifold of images," in *CVPR*, 2010, pp. 2933–2939.
- [20] M. Miller and L. Younes, "Group actions, homeomorphisms and matching: A general framework," *Int. J. Comput. Vis.*, vol. 41, pp. 61–84, 2001.
- [21] S. Kurtk *et al.*, "Parameterization-invariant shape comparisons of anatomical surfaces," *IEEE Trans. Med. Imag.*, vol. 30, no. 3, pp. 849–858, Mar. 2011.
- [22] M. Belkin and P. Niyogi, "Using manifold structure for partially labeled classification," in *NIPS*, 2002, pp. 953–960.
- [23] G. Wu, H. Jia, Q. Wang, and D. Shen, "Sharpmean: Groupwise registration guided by sharp mean image and tree-based registration," *NeuroImage*, vol. 56, no. 4, pp. 1968–1981, 2011.
- [24] X. Zhu, Semi-supervised learning literature survey Dept. Comput. Sci., Univ. Wisconsin, Madison, WI, Tech. Rep. 1530, 2005.
- [25] M. Belkin and P. Niyogi, "Semi-supervised learning on Riemannian manifolds," *Mach. Learn.*, vol. 56, no. 1, pp. 209–239, 2004.
- [26] J. Munkres, *Topology*. Prentice Hall, 2000.
- [27] D. Mumford, J. Fogarty, and F. Kirwan, *Geometric Invariant Theory*. New York: Springer, 1994.
- [28] L. Hagen and A. Kahng, "New spectral methods for ratio cut partitioning and clustering," *IEEE Trans. Computer-Aided Design Integr. Circuits Syst.*, vol. 11, no. 9, pp. 1074–1085, Sep. 1992.
- [29] J. Shi and J. Malik, "Normalized cuts and image segmentation," *IEEE Trans. Pattern Anal. and Machine Intell.*, vol. 22, no. 8, pp. 888–905, 2000.
- [30] V. Vapnik, *Statistical Learning Theory*. New York: Wiley, 1998.
- [31] T. Cormen, C. Leiserson, R. Rivest, and C. Stein, *Introduction to Algorithms*. Cambridge, MA: MIT Press, 2001.
- [32] H. Karcher, "Riemannian centers of mass and mollifier smoothing," *Commun. Pure Appl. Math.*, vol. 30, pp. 509–541, 1977.
- [33] A. Boyd and L. Vandenberghe, *Convex Optimization*. Cambridge, U.K.: Cambridge Univ. Press, 2004.
- [34] P. Fletcher, S. Venkatasubramanian, and S. Joshi, "Robust statistics on Riemannian manifold via the geometric median," in *CVPR*, 2008, pp. 1–8.
- [35] B. Avants, N. Tustison, G. Song, P. Cook, A. Klein, and J. Gee, "A reproducible evaluation of ants similarity metric performance in brain image registration," *Neuroimage*, vol. 54, no. 3, pp. 2033–2044, 2011.